SCIENCE CHINA
Life Sciences

• RESEARCH PAPER •

July 2014 Vol.57 No.7: 698–709
doi: 10.1007/s11427-014-4680-8

The *in vitro* and *in vivo* anti-tumor effects of MTX-Fe_3O_4-PLLA-PEG-PLLA microspheres prepared by suspension-enhanced dispersion by supercritical CO_2

CHEN AiZheng[1,2*], DANG TingTing[1], WANG ShiBin[1,2*], TANG Na[1], LIU YuanGang[1,2] & WU WenGuo[1,2]

[1]*College of Chemical Engineering, Huaqiao University, Xiamen 361021, China;*
[2]*Institute of Biomaterials and Tissue Engineering, Huaqiao University, Xiamen 361021, China*

Received September 9, 2013; accepted February 26, 2014; published online June 13, 2014

The *in vitro* and *in vivo* anti-tumor efficacy of methotrexate-loaded Fe_3O_4-poly-*L*-lactide-poly(ethylene glycol)-poly-*L*-lactide magnetic composite microspheres (MTX-Fe_3O_4-PLLA-PEG-PLLA MCMs, MMCMs), which were produced by co-precipitation (C) and microencapsulation (M) in a supercritical process, was evaluated at various levels: cellular, molecular, and integrated. The results at the cellular level indicate that MMCMs (M) show a better anti-proliferation activity than raw MTX and could induce morphological changes of cells undergoing apoptosis. At the molecular level, MMCMs (M) lead to a significantly higher relative mRNA expression of bax/bcl-2 and caspase-3 than MMCMs (C) at 10 μg mL^{-1} (P<0.01); and the pro-caspase-3 protein expression measured by Western blot analysis also demonstrates that MMCMs (M) can effectively activate pro-caspase-3. At the integrated level, mice bearing a sarcoma-180 tumor are used; *in vivo* anti-tumor activity tests reveal that MMCMs (M) with magnetic induction display a much higher tumor suppression rate and lower toxicity than raw MTX. Pharmacokinetic studies show that MMCMs (M) with magnetic induction significantly increase the accumulation of MTX in the tumor tissue compared with the other treatments. These results suggest that the MMCMs (M) prepared by the SpEDS process have great potential to play a positive role in the magnetic targeted therapy field.

methotrexate, magnetic microsphere, anti-tumor, biological effectiveness

Citation: Chen AZ, Dang TT, Wang SB, Tang N, Liu YG, Wu WG. The *in vitro* and *in vivo* anti-tumor effects of MTX-Fe_3O_4-PLLA-PEG-PLLA microspheres prepared by suspension-enhanced dispersion by supercritical CO_2. Sci China Life Sci, 2014, 57: 698−709, doi: 10.1007/s11427-014-4680-8

Cancer is a leading cause of death worldwide, mainly because malignant tumor cells are highly genetically unstable and excessively proliferative, and they have an enhanced ability to invade cells and metastasize in comparison to normal cells [1]. In the treatment of several cancers, medical research has given considerable attention to increasing the local drug concentration around tumor tissue and minimizing the systemic side-effects on normal tissues or cells.

Recently, with the development and synergy of materials innovation and nanotechnology fuelling the therapy, various anticancer drug carriers have been advancement of drug delivery systems for cancer developed, such as polymer nanoparticles [2], nanoparticle suspensions [3], liposomes [4], dendritic macromolecules [5], inorganic nanoparticles [6], and functionalized carbon nanotubes [7]. Furthermore, in order to increase the targeting efficiency, increasing attention has been given to targeted drug delivery systems (TDDS). The applications of the enhanced permeability and retention (EPR) effect [8], antibodies [9], folate [10], and cancer cell homing peptides [11] in TDDS have been reported; the physicochemical methods represent another

*Corresponding author (email: azchen@hqu.edu.cn; sbwang@hqu.edu.cn)

promising way to achieve a targeted delivery by some stimulus, such as temperature [12], pH [13], magnetic field [14], or mutual combination [15,16]. Among them, magnetic TDDS is used extensively to improve the targeting property by application of an external magnetic field; consequently, the therapeutic effects of drugs can be enhanced.

As a new drug formulation candidate for biomedical applications, its safety and effectiveness must be evaluated before entering the clinical trials stage because of the potential alteration in the biological effects of the drug to be transported. Traditionally, the evaluation of the effectiveness of a drug formulation has been focused on cell viability [17]. However, the evaluation at a cellular level is not comprehensive. For the sake of harvesting more reliable results, evaluating the effectiveness of the formulations at omnidirectional levels is necessary [18,19]. At a cellular level, evaluation has mainly involved the detection of cell apoptosis by various methods with integrated advantages [20,21]. At a molecular level, the expressions of the apoptosis-related genes and proteins [22,23] have been the main focus of investigation. Evaluation at an integrated level has mainly examined anti-tumor activity and pharmacokinetics [24,25]. With the rapid development of life science and special features of formulations, some of the new evaluation methods should be adopted [26].

In our previous studies [27,28], using a process of SpEDS, MTX-Fe_3O_4-PLLA-PEG-PLLA magnetic composite microspheres were produced by co-precipitation and microencapsulation processes [MMCMs (C/M)], and the biocompatibility of Fe_3O_4-PLLA-PEG-PLLA MCMs was evaluated. In this work, based on the above results, the effectiveness of MMCMs (C/M) was evaluated at three levels: cellular, molecular, and integrated.

1 Materials and methods

1.1 Materials and cell culture

A schematic diagram of the SpEDS apparatus and the preparation process was shown in our previous study [27]. In this work, theoretical drug loads were set at 10%, and the corresponding drug loads of MMCMs (C) and MMCMs (M) were 11.72%±0.00% and 5.06%±0.01%, respectively. These microspheres were further treated through cobalt-60 radiation sterilization.

Alamar blue was purchased from Invitrogen (USA). A normal/apoptotic/necrotic cell detection kit and a BCA protein estimation kit were purchased from Kaiji Bio-Company (Nanjing, China). A cell cycle and apoptosis analysis kit, cell lysis buffer for Western blot analysis and immunoprecipitation (IP), phenylmethylsulfonyl fluoride (PMSF), and BeyoECL Plus were purchased from the Beyotime Institute of Biotechnology (Jiangsu, China). The RNAiso Plus, Prime Script™ RT reagent kit and SYBR Premix Ex Taq™ II (Tli RNaseH Plus) were purchased from TaKaRa Bio Ltd. (Dalian, China). All other chemicals were of analytical grade.

MG-63 cells (a human osteosarcoma cell line) and S-180 cells (a mouse sarcoma cell line) were purchased from the Committee of Type Culture Collection of the Chinese Academy of Sciences (Shanghai, China). MG-63 cells were cultured in Dulbecco's Minimum Essential Medium (DMEM, Gibco, USA) and S-180 cells were grown in RPMI1640 Medium (Gibco, USA) supplemented with 10% heat-inactivated fetal bovine serum (Gibco, USA) and 1% antibiotics (100 U mL^{-1} penicillin and 0.1 mg mL^{-1} streptomycin) (Hyclone, USA). The cells were cultured in a humidified incubator at 37°C (95% humidity, 5% CO_2). Kunming mice were purchased from the Slac Laboratory Animal Co. Ltd. (Shanghai, China). Animals were kept in a facility and had free access to food and water, under a 12 h light/dark cycle.

1.2 Cellular level evaluation

1.2.1 In vitro anti-tumor assay

The anti-tumor activity of MMCMs against MG-63 cells was examined by a cell viability test using the Alamar blue proliferation kit. 100 μL of cell suspension was seeded in 96-well plates (Corning, USA) at a density of 3000 cells/well and incubated for 24 h to allow cell attachment. The culture medium was then replaced by 200 μL of MTX, MTX nanoparticles, or MMCMs (C/M) suspension (dispersed in DMEM with MTX concentrations of 0.01, 0.1, 1, 10, and 100 μg mL^{-1}) for 72 h. In addition, a time-dependent manner survey was performed: cells were incubated with 200 μL of MTX, MTX nanoparticles, MMCMs (C/M) (MTX concentrations of 3 μg mL^{-1}) or MCMs suspension (blank microspheres, polymer concentration of 100 μg mL^{-1}) for 24, 48, 72, 120, and 168 h. Controls were cultivated under the same conditions with fresh medium. In order to negate the effects of medium evaporation, only the internal 60 wells were employed for testing and the outer wells had 200 μL of PBS added to them. At the determined time, assays were implemented according to the manufacturer's instructions. Briefly, the control and test samples were removed, and the cells were rinsed twice with PBS, then 100 μL of 10% (v/v) Alamar blue solution was added to each well. After incubation for 4 h, Alamar blue fluorescence was determined at 570 nm, using 600 nm as a reference wavelength by a microplate reader (Spectra Max M5, Molecular Devices, USA). The spectrophotometer was calibrated to zero absorbance using culture medium without cells (blank). Cell viability and half inhibitory concentration (IC_{50}, modified Kou-type method) were calculated with the following formula:

$$\text{Cell viability } (\%)=[A_{570-600}(\text{sample})-A_{570-600}(\text{blank})]/[A_{570-600}(\text{control})-A_{570-600}(\text{blank})],$$

$$\lg IC_{50}=Xm-I(P-(3-Pm-Pn)/4).$$

Here, *Xm* is lg(maximum dose); *I* is lg(maximum dose/adjacent dose); *P* represents sum of positive response rate; *Pm* represents the largest positive response rate; *Pn* represents the smallest positive response rate; positive response rate=1−cell viability. Data were presented as mean± standard deviation (SD) with 6-well repeats.

1.2.2 Morphological observation

The morphologies of apoptotic and necrotic cells were detected by AO-EB fluorescence staining. Exponential-growth-phase MG-63 cells were seeded at a final concentration of 1×10^5/well in 24-well plates and cultured for 24 h, after which the culture medium was removed and 1 mL of the test sample solutions was added. After 48 h of incubation, according to the instructions of the normal/apoptotic/necrotic cell detection kit, the cells were harvested with 0.25% trypsin and re-suspended in 1 mL of DMEM medium. After the cells were washed twice with PBS and re-suspended in 100 μL of PBS, 25 μL of the cell suspension was mixed with 1 μL of a mixed dyes reagent for 2–3 min in darkness, then 10 μL of samples was placed on a microscope slide and visualized under a fluorescence microscope (Leica, German) using a blue filter.

1.2.3 Cell cycle assay

The cell cycles were determined by flow cytometry with PI staining according to the cell cycle and apoptosis analysis kit. A total of 8×10^5 MG-63 cells were seeded in 6-well plates; after being subcultured for 24 h, the medium was changed to an incomplete medium for 12 h for cell cycle synchronization, and then the cells were treated with 2 mL of the test sample solutions for 48 h. Three dishes with different concentrations were prepared, and then the adhesive cells and suspended cells were harvested, pooled, and pelleted. After being washed twice with PBS, the cells were fixed in ice-cold 70% (v/v) ethanol for 24 h at 4°C. Before analysis, the cells were washed with 1 mL of PBS and filtered through a 200 mesh sieve, centrifuged, suspended in 0.5 mL of staining buffer containing RNase A and PI, and then incubated at 37°C for 30 min in darkness. The cells were analyzed with a fluorescence excitation wavelength of 480 nm using a Cell Lab Quanta SC flow cytometer (Beckman Coulter).

1.3 Molecular level evaluation

1.3.1 Real-time reverse transcription polymerase chain reaction (real-time RT-PCR) assay

The mRNA expressions of bcl-2, bax, and caspase-3 genes were detected by real-time RT-PCR. After 1×10^6 MG-63 cells were seeded in 6-well plates and incubated for 24 h at 37°C, the test sample solutions were added to each group, with a further incubation for 72 h. The intracellular total RNA was extracted with Trizol reagent, and the purity and concentration were measured by ultraviolet spectrophotometry; the quality was checked by agarose gel electrophoresis. The Prime Script® RT reagent Kit was then used to construct the cDNA library, which was further accessed as the template of the real-time PCR. The specific primer and β-actin (internal control) sequences (Shanghai Sangone Company, China) are listed in Table 1. Real-time PCR reactions were performed using a SYBR Premix Ex Taq™ II Kit on the ABI Prism®7500 system. Each reaction was run in a 20 μL mixture containing 10 μL of SYBR Premix Ex Taq (2×), 0.8 μL of each primer (10 μmol L^{-1}), 2 μL of cDNA, 0.4 μL of ROX Reference Dye II (50×), and 6 μL of ddH_2O. A two-step real-time PCR cycle was carried out; the steps included an initial predenaturation by heating to 95°C for 30 s, followed by 40 cycles involving denaturation at 95°C for 5 s, and annealing and elongation at 60°C for 34 s. The fluorescence signal was harvested at the end of each cycle. Melting curve analysis was used to confirm the specificity of the products. Results were analyzed by the $2^{-\Delta\Delta C_T}$ method [29].

1.3.2 Western blot assay

The expression of pro-caspase-3 protein in MG-63 cells was detected by Western blot analysis. The cells were first treated according to the same procedure described for the real time RT-PCR assay, and then the cell lysates were prepared following harvesting of the cells in cell lysis buffer for Western blot analysis and IP. The protein was quantified by a BCA protein estimation kit, and 100 μg of proteins per lane was separated by 12% sodium dodecyl sulfate poly-

Table 1 Primer sequences for the real-time RT-PCR

	Name	Primer sequences (5′–3′)	Amplification length (bp)
Bcl-2	BCL2-F1	GTGGATGACTGAGTACCTGAACC	124
	BCL2-R1	AGACAGCCAGGAGAAATCAAAC	
Bax	BAX-F1	CCCGAGAGGTCTTTTTCCGAG	155
	BAX-R1	CCAGCCCATGATGGTTCTGAT	
Caspase-3	CASP3-F1	ATCACAGCAAAAGGAGCAGTTT	214
	CASP3-R1	ACACCACTGTCTGTCTCAATGC	
β-actin	F305	CTGGGACGACATGGAGAAAA	564
	R868	AAGGAAGGCTGGAAGAGTGC	

acrylamide gel electrophoresis (SDS-PAGE) and transferred electrophoretically to poly(vinylidene fluoride) (PVDF) membranes. The membranes were blocked with TBST (100 mmol L^{-1} Tris-HCl pH 7.5, 150 mmol L^{-1} sodium chloride, 0.05% Tween-20) containing 5% skimmed milk powder for 60 min. Then the blots were incubated overnight at 4°C with TBST buffer containing appropriate amounts of primary antibodies: caspase-3 (1:400; Boster, China) and β-actin (1:3000; Bioworld Technology, USA). The blots were then washed three times with TBST and incubated with anti-rabbit secondary antibody conjugated with horseradish peroxidase (HRP) (1:1000; Beyotime, China). The membranes were washed three times again, and the protein signals were detected by an ECL plus kit using an image analyzer (Kodak Image Station 4000 MM Pro). Densitometric analysis was performed using the Quantity One software version 4.6.2.

1.4 Integrated level evaluation

1.4.1 In vivo anti-tumor activity

In vivo anticancer activity against sarcoma-180 (S-180) solid tumors was evaluated in KM mice. Viable S-180 tumor cells ($(1–3)\times10^6$) were propagated in the intraperitoneal cavity of adult KM mice by intraperitoneal injection. The S-180 ascites tumor cells were then harvested on the eighth day and suspended at $(1–2)\times10^7$ cells mL^{-1} in stroke-physiological saline solution; 0.2 mL of this cell suspension was inoculated subcutaneously into the right armpit of the mice using a 1.0 mL syringe.

When the tumor volumes reached about 300 mm^3 (about six days after tumor inoculation), the mice were randomly divided into seven groups (six mice/group). Groups 1, 2, and 3 were injected with PBS (control), MCMs, and MTX, respectively. Groups 4–5 and 6–7 were treated with MMCMs (C) and MMCMs (M), respectively. For groups 5 and 7, the tumors were exposed to a 0.4 T magnetic field produced by a permanent magnet with the help of adhesive tapes immediately after administration [30]. The dose of MTX was 10 mg kg^{-1} drug equivalent in all experimental mice. Each test compound was administered via tail vein injection every other day for 10 d (five times). Body weight and tumor volume were measured at defined drug administration periods, and tumor volume was calculated based on the following equation: major axis×(minor axis)^2×1/2. Twenty-four hours after the last administration, the animals were sacrificed by cervical dislocation, and the tumor mass was harvested and weighed. The inhibitory rate of the tumor was calculated by the following formula:

$$\text{Inhibition ratio } (IR, \%)=[(A-B)/A]\times100\%,$$

where A is the average tumor weight of the negative control and B is that of the treated group. At the end of the experiment, the tumor and small intestine tissues were fixed with 10% formaldehyde for 24 h and embedded in paraffin. Each section was cut to 5 μm, processed for routine hematoxylin and eosin (H&E) and Prussian blue staining, and photographed under an Olympus microscope (BX-51).

1.4.2 Pharmacokinetics assay

Pharmacokinetics studies were performed using S-180-bearing KM mice models. In total, 84 mice were randomly assigned to three groups (28 mice per group): MTX solution, MMCMs (M), and MMCMs (M) (with magnetic induction). The mice were treated with a single tail vein injection at an MTX dose of 10 mg kg^{-1} for each mouse. For the pharmacokinetic experiment, at the designated times (5, 15, and 30 min and 1, 2, 4 and 12 h) after administration, blood samples were taken from the retro orbital plexus, and plasma was isolated by centrifugation (10 min at 3000 r min^{-1}) and stored at −20°C. The mice were then sacrificed and the major tissues, including the tumor and the liver, were collected, washed with saline, blotted dry with filter paper, wrapped with tinfoil, and stored at −80°C for assay.

For the plasma sample preparation, 200 μL of the plasma sample was added to 100 μL of saline and 100 μL of perchloric acid (20%). For the tissue sample preparation, 300 μL of tissue homogenate was added to 300 μL of perchloric acid. The sample mixture was thoroughly vortex-mixed for 5 min, followed by centrifugation at 10000 r min^{-1} for 10 min. The supernatant was then centrifuged again, filtered through a 0.22 μm filter membrane, and transferred to a fresh tube. 20 μL of this solution was injected into the high performance liquid chromatography (HPLC) (LC-2000, Japan) system for analysis, with experimental conditions as follows: C18 column (150 mm×4.6 mm, pore size 5 μm); the mobile phase, 3% glacial acetic acid: acetonitrile (90:10, v/v); flow rate, 1.0 mL min^{-1}; column temperature, 35°C; measured wavelength, 303 nm. Non-compartmental pharmacokinetic analysis was performed using the software Winnonlin. The animal experiments were carried out in accordance with the guidelines issued by the Ethical Committee of Huaqiao University.

1.5 Statistical analysis

Data were expressed as mean±SD. Results were analyzed by one-way ANOVA. $P<0.05$ was considered statistically significant and $P<0.01$ was considered highly statistically significant.

2 Results and discussion

2.1 The effect of MMCMs (C/M) on MG-63 cell growth *in vitro*

Prior to *in vivo* evaluation, the anti-tumor activity of the

MTX formulations at the cellular level was studied by means of a colorimetric microculture assay (Alamar blue assay), and based on previous reports [31], we chose MG-63 cells as the model of cancer cells. The IC_{50} values of MTX, MTX nanoparticles, and MMCMs (C/M) were calculated to be 17.99, 14.03, 6.07, and 8.88 μg mL^{-1}, respectively, which suggest that MMCMs (C/M) had an enhanced anti-tumor activity compared with raw MTX, showing a smaller IC_{50} than raw MTX. As shown in Figure 1, the cell viability of MG-63 cells incubated with MCMs was close to 100% during the experimental period. It was observed that exposure of MG-63 cells to MTX nanoparticles significantly decreased cell viability after four days in comparison with exposure to raw MTX over the same period (P<0.01). In comparison with the response to raw MTX, the cell viability with MMCMs (C/M) kept decreasing after three days (P<0.01); furthermore, values for cell viability with MMCMs (M) were the lowest on the seventh day (P<0.01). The results indicate that MCMs had almost no effect on cell proliferation, and this was consistent with a previous report [32]. MTX nanoparticles could induce a lower cell viability than raw MTX, which could be explained by the fact that a significant increase in the dissolution rate of MTX nanoparticles occurred to increase the bioavailability of MTX [33]. Furthermore, compared with MMCMs (C), MMCMs (M) had an enhanced anti-cancer efficacy on MG-63 cells in a time-dependent manner, which could be attributed to the better sustained-release property. The optical micrographs of MG-63 cells incubated with different MTX formulations were also consistent with this result; it could be seen that the attachment ability of the cells incubated with MMCMs (C/M) became poor and a large number of cells became deformed and brushed off (Figure S1 in Supporting Information).

The results suggest that MMCMs (M) had a better anti-proliferation activity than the other formulations. However, the cell viability in the MMCMs (M) group was not significantly decreased when compared with previous reports [34,35]. This can be explained that the concentration of MTX (3 μg mL^{-1}) was chosen according to achievable plasma drug levels in humans, and it was lower than the level of IC_{50}. We believe that the cell viability will be significantly decreased when the concentration of MTX is increased with the increasing in drug load of MMCMs (M).

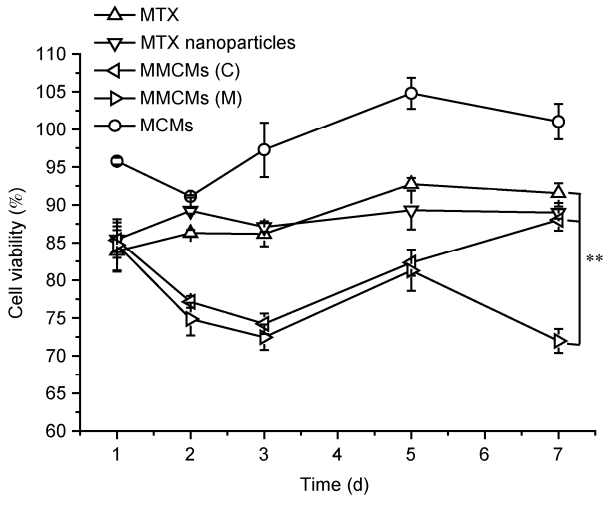

Figure 1 Cell viability of MG-63 cells incubated with 3 μg mL^{-1} of MTX, MTX nanoparticles, and MMCMs (C/M), and 100 μg mL^{-1} of MCMs for 1, 2, 3, 5, and 7 d at 37°C.

2.2 The effect of MMCMs (C/M) on MG-63 cell morphology

AO-EB dual staining is commonly used to study the death pattern of cells, distinguishing the viable cells, early/medium/late apoptotic cells, and necrotic cells [36]. It is known that AO is a cell-permeable dye that intercalates into DNA and emits green fluorescence, while EB enters cells with disrupted membrane integrity and intercalates into RNA and DNA, appearing orange in color. As shown in Figure 2, after AO-EB staining, the control cells (A) and cells treated with MCMs (B) emitted uniformly green fluorescence and almost no death or apoptosis was observed. In contrast, the cells treated with MTX (C) showed the presence of non-uniform green patches of fragmented and condensed chromatin, which are the characteristics of early apoptosis. However, some of the cells incubated with the MTX nanoparticles (D) and MMCMs (C/M) (E/F) exhibited obvious orange patches of fragmented and condensed chromatin, nuclear fragmentation, or apoptotic bodies, all of which are characteristics of apoptotic programmed cell death. Therefore, the above observations demonstrated that MMCMs (C/M) could dramatically induce apoptosis of MG-63 cells [37], which was also supported by the results obtained from the effect of MMCMs (C/M) on MG-63 cell growth *in vitro*.

2.3 The effect of MMCMs (C/M) on the MG-63 cell cycle

A quantitative evaluation of MMCMs-induced cell death was carried out through cell cycle analysis using PI staining, which was intended to reflect cell proliferation at various stages of cells. PI is a kind of double-stranded DNA fluorescent dye; their combination can produce fluorescence, which is detected by flow cytometry, and thus the DNA contents are calculated [38]. The effects of different kinds of MTX formulations on the cycle of MG-63 cells over 48 h are shown in Figure 3, which shows an increase in the S phase compared with the control (P<0.01) and also a decrease in the G_0/G_1 phase. It was observed that the S phase with 3 μg mL^{-1} of MMCMs (C/M) increased up to 46.83% and 48.18%, respectively, while 5.91% in the control. At the same time, the G_0/G_1 phase decreased from 78.29% in the control to 36.36% and 34.62%, respectively. There were no

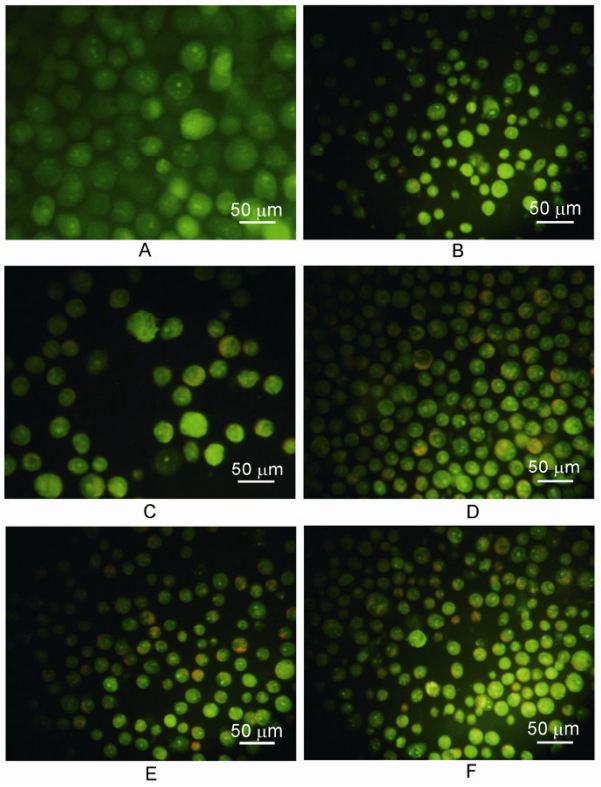

Figure 2 AO-EB dual staining of MG-63 cells after culturing with (A) fresh medium (control); (B) 100 μg mL^{-1} of MCMs; (C) MTX; (D) MTX nanoparticles; (E) MMCMs (C); and (F) MMCMs (M) (with 3 μg mL^{-1} of MTX) for 48 h (×400).

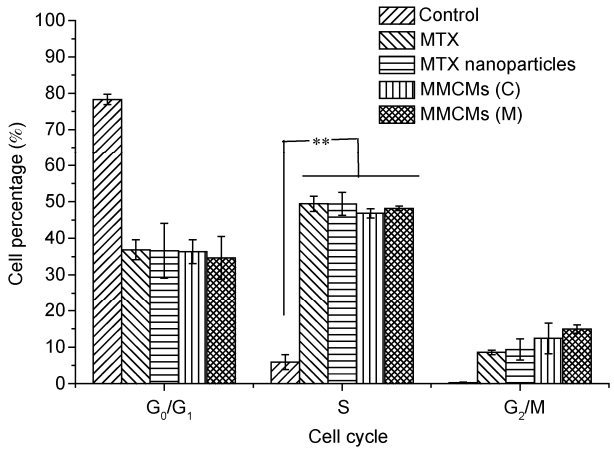

Figure 3 Effects of different MTX formulations on the cycle of MG-63 cells over 48 h.

significant statistical differences (P>0.05) between the effects of MTX and MMCMs (C/M) in the S phase, which indicated that MMCMs (C/M) did not decrease efficacy and arrest the cell cycle in the S phase. As demonstrated by other published data, MTX is an S phase specific drug, which generally produces growth arrest in the S phases of the cell cycle [39].

2.4 The effect of MMCMs (C/M) on the expression of mRNA and protein levels

The ratio of the pro-apoptotic (bax) to anti-apoptotic (bcl-2) molecules is crucial in apoptosis [40]. Inhibition of the expression of bcl-2 will result in the activation of caspase-3, which is a key factor of the Caspase family and plays a very important role in cell apoptosis. Therefore, we studied the effect of MMCMs (C/M) on bcl-2, bax, and caspase-3 mRNA and pro-caspase-3 protein expression. The results of real-time RT-PCR are shown in Figure 4A and B. The relative expression levels of bax/bcl-2 and caspase-3 mRNA in MTX were higher than those of the other treatments. The expression levels of MMCMs (M) were much higher than those of MMCMs (C), and the difference was statistically significant (P<0.01). The changes in the transcriptional profiles of the caspase-3 gene were further reconfirmed by Western blot analysis. Potent apoptosis markers such as pro-caspase-3 protein were all found to be significantly decreased in response to the test chemicals [41]. As shown in Figure 5A and B, the pro-caspase-3 protein in the 10 μg mL^{-1} of MMCMs (M) was the lowest among all of the formulations. These results demonstrate that MMCMs (M) had a pro-apoptotic effect on MG-63 cells, which could effectively increase the gene expression of bax/bcl-2 and caspase-3 and activate the protein expression of pro-caspase-3 more effectively than MMCMs (C).

2.5 The effect of MMCMs (C/M) on tumor growth *in vivo*

To investigate the anti-tumor efficacy of MMCMs (C/M) *in vivo*, we here selected S-180 tumor-bearing mice as an animal model because it has been one of the classical solid tumor models for a long time [42]. Tumor volumes, weights, and inhibitory rates were used as evaluating indicators of efficacy and are shown in Figure 6 and Table 2. Relative to PBS, MCMs resulted in a similar increase in tumor volume at all-time points after treatment, with a relatively low IR (10%) (P>0.05). However, the other groups showed a tumor growth suppression activity. When the mice were treated with MTX alone, a mean tumor volume of 1260±180 mm^3 after the last dosing (P<0.01) and a relatively high *IR* (49%) were observed. Under a magnetic field of 0.4 T, MMCMs (C) and MMCMs (M) showed mean tumor volumes of 800±170 (P<0.05) and 560±40 mm^3 (P<0.01) after the last dosing, respectively, as well as a high IR (54% and 64%, respectively). Furthermore, the difference between the effects of MMCMs (C) and MTX after the last dosing was significant (P<0.05), and the difference between the effects of MMCMs (M) and MTX (P<0.01) after the last dosing was highly significant. This clearly indicates that MMCMs (M) under magnetic induction could significantly improve the anti-tumor activity of MTX.

The representative microphotographs of H&E-stained

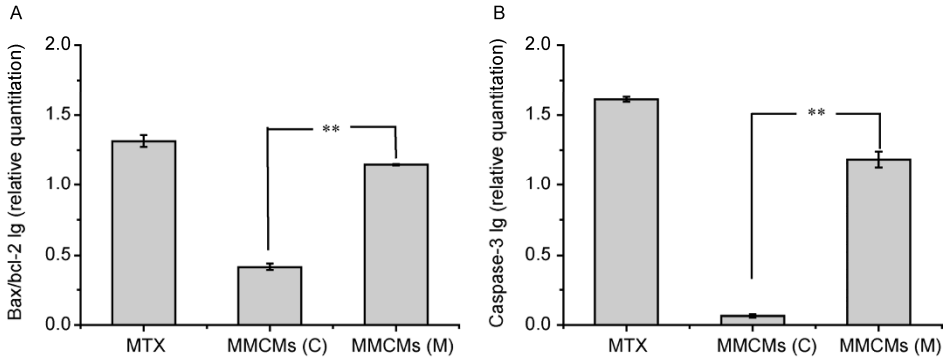

Figure 4 Expression of bax/bcl-2 (A) and caspase-3 (B) mRNA relative expression in MG-63 cells after 72 h of incubation with experimental groups. **, $P<0.01$.

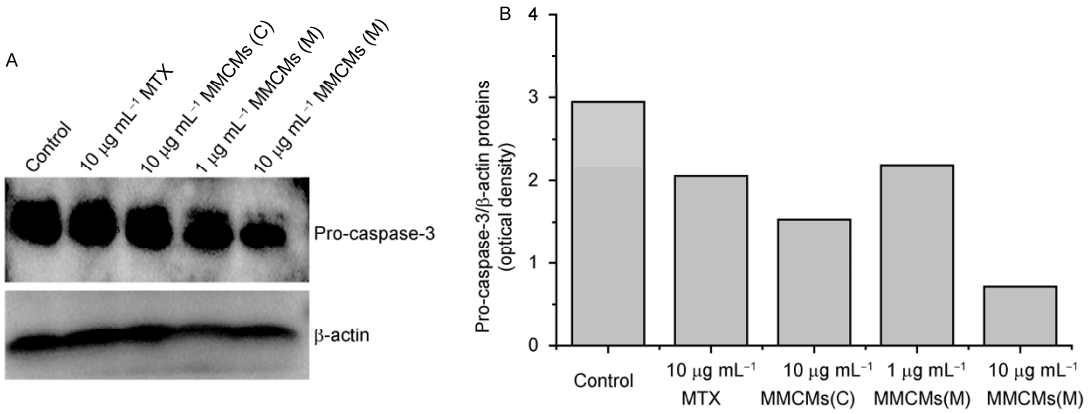

Figure 5 Effects of MTX and MMCMs (C/M) on the activation of pro-caspase-3 in MG-63 cells by Western blots. Proteins were isolated from MG-63 cells incubated with the control, 10 μg mL^{-1} of MTX, 10 μg mL^{-1} of MMCMs (C), 1 μg mL^{-1} of MMCMs (M), and 10 μg mL^{-1} MMCMs (M) after 72 h. A, Expression levels of pro-caspase-3 and β-actin proteins. B, Optical density ratio of pro-caspase-3/β-actin analysis.

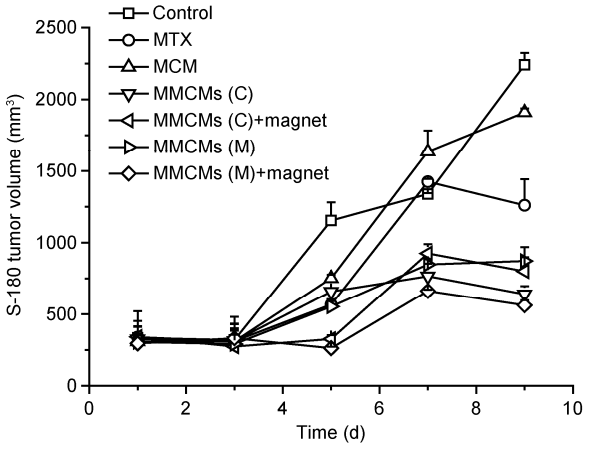

Figure 6 The curves of volume change of S-180 solid tumors treated with MMCMs.

sections of S-180 tumor cells are shown in Figure 7. Figure 7A reveals the presence of typical tumor cells with good growth in the S-180 control group (PBS), where the nuclei were dyed bright blue by hematoxylin, the cytoplasm was dyed in different shades of pink by eosin, and tumor cells were dense. However, when the mice were treated with MTX and MMCMs (C) subjected to magnetic induction, large pink areas and intercellular space can be seen, indicating necrosis (Figure 7B and C) [43]. Furthermore, MMCMs (M) under magnetic induction showed more extensive necrotic areas than the other formulations (Figure 7D). This was consistent with the results of inhibitory rates. Meanwhile, tumor tissues were also observed by Prussian blue staining (Figure S2 in Supporting Information). There were no blue iron particles in the PBS and MTX groups. The MMCMs (C) group showed only small amounts of blue iron particles under magnetic induction, while the MMCMs (M) group showed a lot of blue iron particles under magnetic induction. The above observations also proved that MMCMs (M) could considerably improve anti-tumor activity under magnetic induction.

The major limitation of cancer chemotherapy is the injury of normal tissue, leading to multiple organ toxicity. MTX is a frequently used cytotoxic agent in the clinic and is associated with acute and chronic neurotoxicity [44]. In order to determine whether MMCMs (C/M) may cause any undesirable side-effects, we assayed the change in body weight [45] and H&E staining of normal tissue (small intestine) [46]

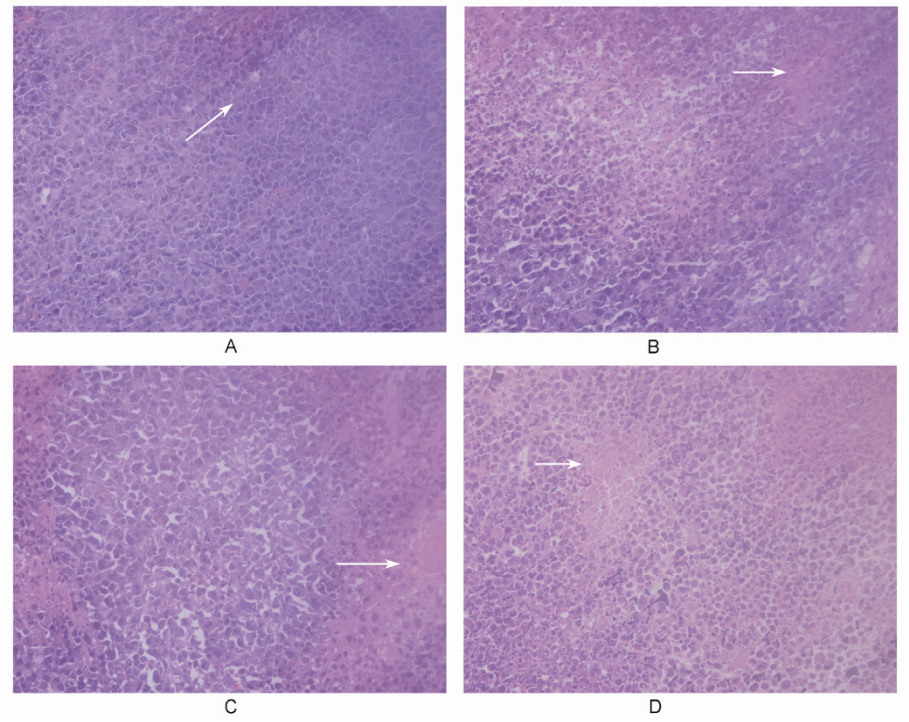

Figure 7 Histopathological analyses of tumors in S-180 tumor-bearing mice (H&E, ×600). A, Blank control. B, MTX. C and D, MMCMs (C/M) at the dose level of 10 mg kg^{-1} under magnetic induction. Thin arrows indicate tumor cells with good growth and thick arrows show tumor necrosis.

Table 2 Inhibitory rate of S-180 solid tumors treated with MMCMs[a)]

Group	Tumor weight (g)	Inhibitory rate (%)
S-180 control (PBS)	2.14±0.26	–
MCMs	1.92±0.15	10.08
MTX	1.09±0.18**	49.32
MMCMs (C)	1.14±0.07**	46.91
MMCMs (C+magnet)	0.99±0.12**	53.68
MMCMs (M)	1.14±0.10**	46.83
MMCMs (M+magnet)	0.77±0.14**	64.21

a) **, $P<0.01$.

as indicators of general toxicity. As presented in Figure 8, relative to PBS injected animals, MTX caused a significant weight loss by day 7 ($P<0.05$). Obviously, MMCMs (C) with magnetic induction resulted in a highly significant weight loss after 7 d ($P<0.01$). In contrast, the MMCMs (M) group under magnetic induction showed a similar increase in mean mice weight at all-time points after treatment ($P>0.05$), suggesting that MMCMs (M) were better tolerated than others. Subsequently, as shown in Figure 9, compared with the control, severe toxicity induced by raw MTX was found, such as inflammation. The findings indicated that MMCMs (M) were associated with fewer harmful side-effects of MTX than MMCMs (C) under magnetic induction. Thus, compared with raw MTX and MMCMs (C), MMCMs (M) were demonstrated to be more curative and less toxic to the mice.

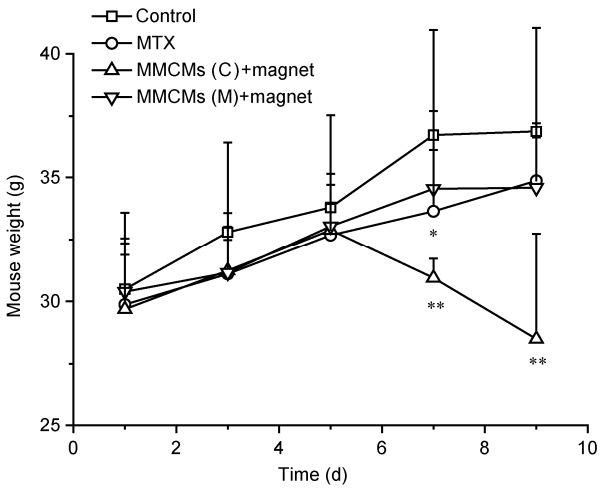

Figure 8 The weight change of S-180 tumor-bearing mice treated with MMCMs.

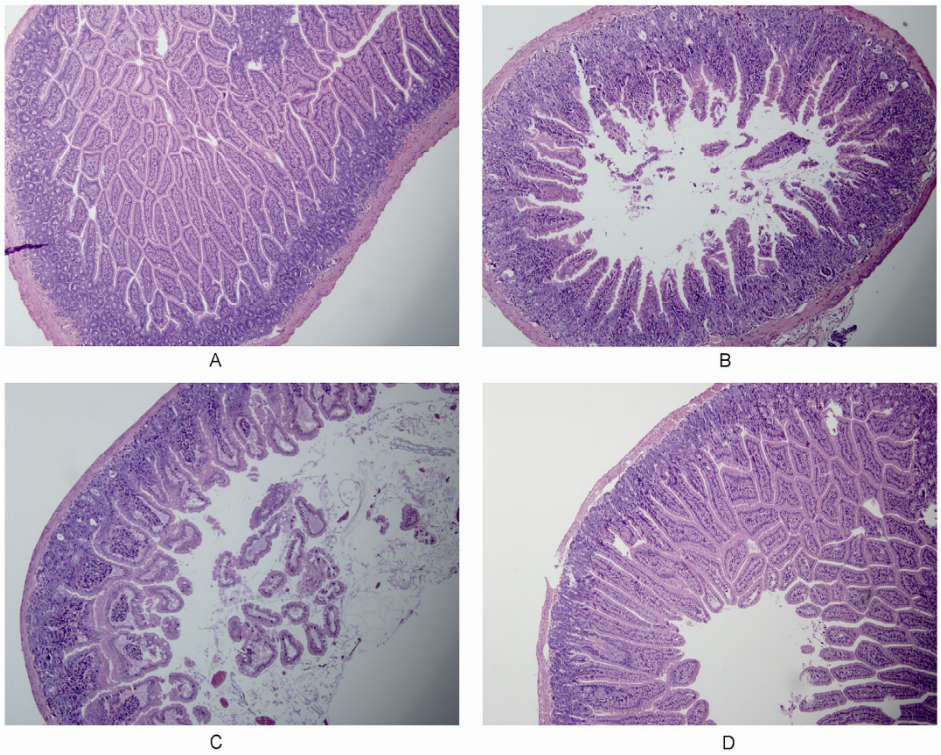

Figure 9 Histopathological analyses of the small intestine in S-180 tumor-bearing mice (H&E, ×300). A, Blank control. B, MTX. C and D, MMCMs (C/M) at the dose level of 10 mg kg^{-1} under magnetic induction.

2.6 Pharmacokinetics study

To further confirm the above results, the pharmacokinetic behavior of MMCMs (M) was assessed in S-180 tumor-bearing mice. After intravenous administration of MTX solution, MMCMs (C), and MMCMs (M) in the presence of a magnetic field, the concentrations of MTX in plasma, liver, and tumor were determined by HPLC. The concentration versus time profiles of these tissues are shown in Figure 10. The corresponding pharmacokinetic parameters in plasma and tissues are listed in Table 3.

As shown in Figure 10, the MTX concentration had a quick decrease after 15 min dosing in the plasma, liver, and tumor. MMCMs (M) under magnetic induction displayed a longer systemic circulation time, especially in the tumor, which suggested a greater *in vivo* targeted effect.

As shown in Table 3, for the MTX solution treatment, the maximum concentrations (C_{max}) in the plasma, liver, and tumor were much higher than those of the other treatments. By application of the external magnetic field, in the MMCMs (M) group, the C_{max} increased significantly from 721 to 979 ng mL^{-1} in the tumor. Furthermore, for time at C_{max} (T_{max}), animals treated with MMCMs (M) under magnetic induction exhibited a delayed time to peak concentration compared with those treated with raw MTX. The terminal phase half-life ($t_{1/2}$) in plasma with the MTX solution treatment was much longer than those with the other treatments. However, under magnetic induction, the $t_{1/2}$ in the tumor was increased up to 1.57-fold compared with MMCMs (M) treatment without the magnetic field and 1.49-fold compared with the MTX solution treatment. The mean retention time (MRT) of the MTX solution treatments in plasma was longer than those of the other treatments. In the tumor, the application of a magnetic field increased the MRT up to 2.07-fold compared with MMCMs (M) treatment without the magnetic field and 1.67-fold compared with the MTX solution treatment. Administration of MMCMs (M) under magnetic induction had the highest AUC_{0-t} (area under the MTX concentration-time curve from time zero to the last measurable concentration) and $AUC_{0-\infty}$ (area under the MTX concentration-time curve from time zero to infinity) compared with those of the other treatments in plasma and tissues. Furthermore, in the tumor, the AUC_{0-t} and $AUC_{0-\infty}$ of the treatment under magnetic induction were increased almost 2.78-fold and 3.63-fold, respectively, compared with treatment without magnetic induction. Comparing systemic clearance (*CL*) and the volume of distribution at steady state (V_{ss}) in the plasma and tissues, administration of MMCMs (M) under magnetic induction significantly decreased the values of *CL* and V_{ss} compared with those of the other treatments. In the tumor, administration of MMCMs (M) under magnetic induction reduced the *CL* to 19.3 mL min^{-1} kg^{-1} and the V_{ss} to 12021 mL kg^{-1}, which were lower values than those of the MTX solution treatment (50.4 mL min^{-1} kg^{-1} and 18863 mL kg^{-1}, respectively) and the MMCMs (M) treatment without mag-

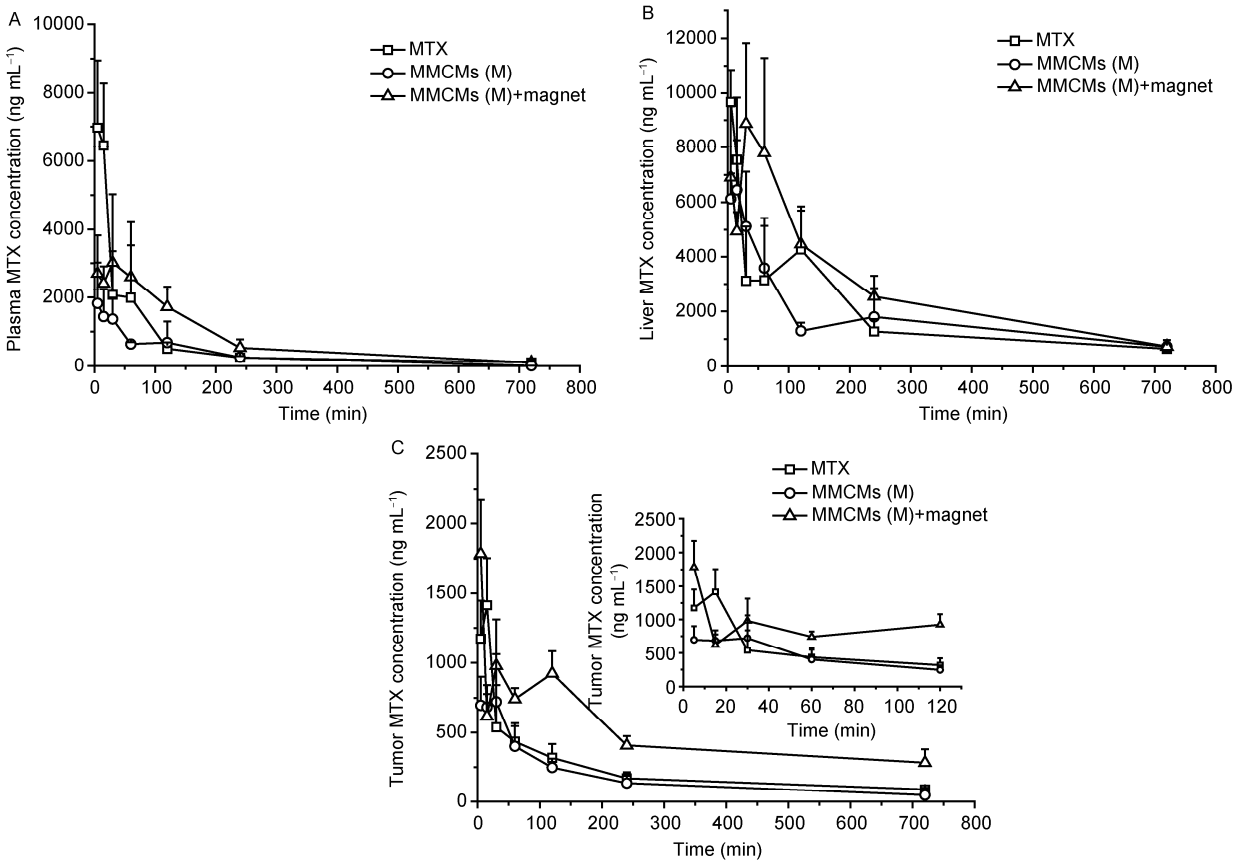

Figure 10 Plasma (A) and tissue (liver (B), tumor (C)) concentration-time curves after intravenous administration of MTX solution and MMCMs (M/M+magnet). The values are expressed as mean±SD (n=4).

Table 3 Pharmacokinetic parameters of MTX in mice plasma and tissues after intravenous administration of MTX solution and MMCMs (M/M+magnet) at the same dose (n=4)[a)]

Group		C_{max} (ng mL^{-1})	T_{max} (h)	$t_{1/2}$ (h)	MRT (h)	AUC_{0-t} h ng mL^{-1}	$AUC_{0-\infty}$ h ng mL^{-1}	CL mL min^{-1} kg^{-1}	V_{ss} (mL kg^{-1})
Plasma	MTX	6973	0.083	4.84	3.50	7214	7952	21.0	4405
	MMCMs (M)	1825	0.083	1.55	2.17	3951	3968	42.0	5467
	MMCMs (M+magnet)	3018	0.500	2.38	2.88	9715	10072	16.5	2862
Liver	MTX	9671	0.083	4.35	5.60	22072	26114	6.38	2146
	MMCMs (M)	6453	0.250	6.02	7.67	20763	26980	6.18	2842
	MMCMs (M+magnet)	8875	0.500	3.98	4.78	33713	37893	4.40	1261
Tumor	MTX	1415	0.250	4.74	6.24	2696	3307	50.4	18863
	MMCMs (M)	721	0.500	4.49	5.02	2063	2372	70.3	21164
	MMCMs (M+magnet)	979	0.500	7.08	10.40	5735	8615	19.3	12021

a) C_{max}, maximum concentration; T_{max}, time at C_{max}; $t_{1/2}$, terminal phase half-life; MRT, mean retention time; AUC_{0-t}, area under the MTX concentration-time curve from time zero to the last measurable concentration; $AUC_{0-\infty}$, area under the MTX concentration-time curve from time zero to infinity; CL, systemic clearance; V_{ss}, the volume of distribution at steady state.

netic induction (70.3 mL min^{-1} kg^{-1} and 21164 mL kg^{-1}, respectively).

Zhu et al. [47] developed MTX-loaded thermosensitive magnetoliposomes, when these liposomes were intravenously administrated in rats, 3.85-fold increase of C_{max} and 9.68-fold increase of MTX accumulation (AUC_{0-t}) in skeletal muscle compared with the absence of magnet were observed. Similar phenomena were also found in our study, the pharmacokinetic behaviors of MTX had a marked difference among the free MTX solution, MMCMs (M) and MMCMs (M) in the presence of magnetic field. MMCMs (M) under magnetic induction increased C_{max} in 1.36-fold

and AUC_{0-t} in 2.78-fold compared with the absence of magnet, and 2.0-fold increase of T_{max} and 2.13-fold increase of AUC_{0-t} compared with free MTX.

The increase in C_{max} indicated that the nanoparticles were effective in increasing the drug absorption, and the delayed T_{max} demonstrated an obvious sustained release of MTX. This was probably because that MMCMs (M) had a good magnetic response and sustained-release effect. Overall, under magnetic induction, MMCMs (M) showed the greatest accumulation of MTX in tumor tissues compared with the other formulations, resulting in an increase in the therapeutic index and safety profile of MTX.

3 Conclusion

To use the MMCMs (C/M) in a drug delivery system, we evaluated their biological effectiveness by measuring their *in vitro* and *in vivo* anti-tumor effects. The anti-tumor efficacy in MG-63 cells was enhanced by MMCMs (M), which have an effective long-term anti-tumor effect and induce cell cycle arrest *in vitro*. In addition, MMCMs (M) increased the gene expression of bax/bcl-2 and caspase-3 and activated the protein expression of pro-caspase-3 more effectively than MMCMs (C). Moreover, MMCMs (M) significantly decreased tumor growth and showed a lower toxicity *in vivo*. The pharmacokinetics study showed that the MTX C_{max}, T_{max}, $t_{1/2}$, and AUC were significantly increased by MMCMs (M) under magnetic induction, while distribution and clearance were decreased, indicating a prolonged circulation time and an increased bioavailability. Based on our present data, MMCMs (M) show great potential for use in the magnetic targeted therapy field.

This work was supported by the National Natural Science Foundation of China (51103049, 31170939), Promotion Program for Young and Middle-aged Teacher in Science and Technology Research of Huaqiao University (ZQN-PY107), Science and Technology Project of Fujian Province (2013Y2002) and Specialized Research Fund for the Doctoral Program of Higher Education (20133501110003).

1 Jemal A, Bray F, Center MM, Ferlay J, Ward E, Forman D. Global cancer statistics. CA Cancer J Clin, 2011, 61: 69–90
2 Li Y, Ji L, Wang G, Song LQ, He B, Li L, Nie Y, Wu Y, Wei ZG. Study on the α-cyclodextrin/poly (ethylene glycol) self-assembly supramolecular nanoparticles for drug delivery. Sci China Chem, 2010, 53: 495–501
3 Yao L, Zhao X, Li Q, Zu Y, Fu Y, Zu B, Meng X, Liu C. *In vitro* and *in vivo* evaluation of camptothecin nanosuspension: a novel formulation with high antitumor efficacy and low toxicity. Int J Pharm, 2012, 423: 586–588
4 Torchilin VP. Recent advances with liposomes as pharmaceutical carriers. Nat Rev Drug Discov, 2005, 4: 145–160
5 Babaei E, Sadeghizadeh M, Hassan ZM, Feizi MAH, Najafi F, Hashemi SM. Dendrosomal curcumin significantly suppresses cancer cell proliferation *in vitro* and *in vivo*. Int Immunopharmacol, 2012, 12: 226–234
6 Qin L, Xue M, Wang W, Zhu R, Wang S, Sun J, Zhang R, Sun X. The *in vitro* and *in vivo* anti-tumor effect of layered double hydroxides nanoparticles as delivery for podophyllotoxin. Int J Pharm, 2010, 388: 223–230
7 Prakash S, Malhotra M, Shao W, Tomaro-Duchesneau C, Abbasi S. Polymeric nanohybrids and functionalized carbon nanotubes as drug delivery carriers for cancer therapy. Adv Drug Deliver Rev, 2011, 63: 1340–1351
8 Maeda H, Bharate GY, Daruwalla J. Polymeric drugs for efficient tumor-targeted drug delivery based on EPR-effect. Eur J Pharm Biopharm, 2009, 71: 409–419
9 Etrych T, Strohalm J, Kovar L, Kabesova M, Rihova B, Ulbrich K. HPMA copolymer conjugates with reduced anti-CD20 antibody for cell-specific drug targeting. I. synthesis and *in vitro* evaluation of binding efficacy and cytostatic activity. J Control Release, 2009, 140: 18–26
10 Ji Z, Lin G, Lu Q, Meng L, Shen X, Dong L, Fu C, Zhang X. Targeted therapy of SMMC-7721 liver cancer *in vitro* and *in vivo* with carbon nanotubes based drug delivery system. J Colloid Interface Sci, 2012, 365: 143–149
11 Yoo MK, Kang SK, Choi JH, Park IK, Na HS, Lee HC, Kim EB, Lee NK, Nah JW, Choi YJ, Cho CS. Targeted delivery of chitosan nanoparticles to Peyer's patch using M cell-homing peptide selected by phage display technique. Biomaterials, 2010, 31: 7738–7747
12 Hossann M, Syunyaeva Z, Schmidt R, Zengerle A, Eibl H, Issels RD, Lindner LH. Proteins and cholesterol lipid vesicles are mediators of drug release from thermosensitive liposomes. J Contr Release, 2012, 162: 400–406
13 Obata Y, Tajima S, Takeoka S. Evaluation of pH-responsive liposomes containing amino acid-based zwitterionic lipids for improving intracellular drug delivery *in vitro* and *in vivo*. J Contr Release, 2010, 142: 267–276
14 Chomoucka J, Drbohlavova J, Huska D, Adam V, Kizek R, Hubalek J. Magnetic nanoparticles and targeted drug delivering. Pharmacol Res, 2010, 62: 144–149
15 Smith CAM, de la Fuente J, Pelaz B, Furlani EP, Mullin M, Berry CC. The effect of static magnetic fields and tat peptides on cellular and nuclear uptake of magnetic nanoparticles. Biomaterials, 2010, 31: 4392–4400
16 Pradhan P, Giri J, Rieken F, Koch C, Mykhaylyk O, Doeblinger M, Banerjee R, Bahadur D, Plank C. Targeted temperature sensitive magnetic liposomes for thermo-chemotherapy. J Contr Release, 2010, 142: 108–121
17 Yu H, Huang Q. Enhanced *in vitro* anti-cancer activity of curcumin encapsulated in hydrophobically modified starch. Food Chem, 2010, 119: 669–674
18 Sloat BR, Sandoval MA, Li D, Chung WG, Lansakara-P DS, Proteau PJ, Kiguchi K, DiGiovanni J, Cui Z. *In vitro* and *in vivo* anti-tumor activities of a gemcitabine derivative carried by nanoparticles. Int J Pharm, 2011, 409: 278–288
19 Guo DD, Xu CX, Quan JS, Song CK, Jin H, Kim DD, Choi YJ, Cho MH, Cho CS. Synergistic anti-tumor activity of paclitaxel-incorporated conjugated linoleic acid-coupled poloxamer thermosensitive hydrogel *in vitro* and *in vivo*. Biomaterials, 2009, 30: 4777–4785
20 Darwich Z, Klymchenko AS, Kucherak OA, Richert L, Mely Y. Detection of apoptosis through the lipid order of the outer plasma membrane leaflet. Biochim Biophys Acta, 2012, 1818: 3048–3054
21 Zagariya AM. A novel method for detection of apoptosis. Exp Cell Res, 2012, 318: 861–866
22 Sun JB, Duan JH, Dai SL, Ren J, Guo L, Jiang W, Li Y. Preparation and anti-tumor efficiency evaluation of doxorubicin-loaded bacterial magnetosomes: magnetic nanoparticles as drug carriers isolated from magnetospirillum gryphiswaldense. Biotechnol Bioeng, 2008, 101: 1313–1320
23 Chakraborty A, Gupta N, Ghosh K, Roy P. *In vitro* evaluation of the cytotoxic, anti-proliferative and anti-oxidant properties of pterostilbene isolated from *Pterocarpus marsupium*. Toxicol In Vitro, 2010, 24: 1215–1228

24 Alexiou C, Jurgons R, Schmid R, Hilpert A, Bergemann C, Parak F, Iro H. *In vitro* and *in vivo* investigations of targeted chemotherapy with magnetic nanoparticles. J Magn Magn Mater, 2005, 293: 389–393

25 Khalil NM, Frabel do Nascimento TC, Casa DM, Dalmolin LF, de Mattos AC, Hoss I, Romano MA, Mainardes RM. Pharmacokinetics of curcumin-loaded PLGA and PLGA-PEG blend nanoparticles after oral administration in rats. Colloid Surface B, 2013, 101: 353–360

26 Jones PS, Jones D. New regulatory framework for cancer drug development. Drug Discov Today, 2012, 17: 227–231

27 Chen AZ, Li L, Wang SB, Lin XF, Liu YG, Zhao C, Wang GY, Zhao Z. Study of Fe_3O_4-PLLA-PEG-PLLA magnetic microspheres based on supercritical CO_2: preparation, physicochemical characterization, and drug loading investigation. J Supercrit Fluid, 2012, 67: 139–148

28 Chen AZ, Lin XF, Wang SB, Li L, Liu YG, Ye L, Wang GY. Biological evaluation of Fe_3O_4-poly(L-lactide)-poly(ethylene glycol)-poly(L-lactide) magnetic microspheres prepared in supercritical CO_2. Toxicol Lett, 2012, 212: 75–82

29 Livak KJ, Schmittgen TD. Analysis of relative gene expression data using real-time quantitative PCR and the $2^{-\Delta\Delta C_T}$ method. Methods, 2001, 25: 402–408

30 Saravanan M, Bhaskar K, Maharajan G, Pillai KS. Ultrasonically controlled release and targeted delivery of diclofenac sodium via gelatin magnetic microspheres. Int J Pharm, 2004, 283: 71–82

31 Decker S, Winkelmann W, Nies B, van Valen F. Cytotoxic effect of methotrexate and its solvent on osteosarcoma cells *in vitro*. J Bone Joint Surg Br, 1999, 81B: 545–551

32 Kang Y, Wu J, Yin G, Huang Z, Liao X, Yao Y, Ouyang P, Wang H, Yang Q. Characterization and biological evaluation of paclitaxel-loaded poly(L-lactic acid) microparticles prepared by supercritical CO_2. Langmuir, 2008, 24: 7432–7441

33 Chen AZ, Li Y, Chau FT, Lau TY, Hu JY, Zhao Z, Mok DK. Application of organic nonsolvent in the process of solution-enhanced dispersion by supercritical CO_2 to prepare puerarin fine particles. J Supercrit Fluid, 2009, 49: 394–402

34 Zhang Y, Thomas TP, Lee KH, Li M, Zong H, Desai AM, Kotlyar A, Huang B, Banaszak Holl MM, Baker Jr JR. Polyvalent saccharide-functionalized generation 3 poly (amidoamine) dendrimer-methotrexate conjugate as a potential anticancer agent. Bioorg Med Chem, 2011, 19: 2557–2564

35 Young KL, Xu C, Xie J, Sun S. Conjugating methotrexate to magnetite (Fe_3O_4) nanoparticles via trichloro-s-triazine. J Mater Chem, 2009, 19: 6400–6406

36 Meng L, Zhang X, Lu Q, Fei Z, Dyson PJ. Single walled carbon nanotubes as drug delivery vehicles: targeting doxorubicin to tumors. Biomaterials, 2012, 33: 1689–1698

37 Wu C, Shi L, Li Q, Jiang H, Selke M, Yan H, Wang X. New strategy of efficient inhibition of cancer cells by carborane carboxylic acid-CdTe nanocomposites. Nanomed Nanotechnol Biol Med, 2012, 8: 860–869

38 Ding X, Zhu FS, Li M, Gao SG. Induction of apoptosis in human hepatoma SMMC-7721 cells by solamargine from *Solanum nigrum* L. J Ethnopharmacol, 2012, 139: 599–604

39 Mohapatra S, Rout SR, Maiti S, Maiti TK, Panda AB. Monodisperse mesoporous cobalt ferrite nanoparticles: synthesis and application in targeted delivery of antitumor drugs. J Mater Chem, 2011, 21: 9185–9193

40 Shi L, Chen J, Yang J, Pan T, Zhang S, Wang Z. MiR-21 protected human glioblastoma U87MG cells from chemotherapeutic drug temozolomide induced apoptosis by decreasing Bax/Bcl-2 ratio and caspase-3 activity. Brain Res, 2010, 1352: 255–264

41 Li X, Zhen D, Lu X, Xu H, Shao Y, Xue Q, Hu Y, Liu B, Sun W. Enhanced cytotoxicity and activation of ROS-dependent c-Jun NH_2-terminal kinase and caspase-3 by low doses of tetrandrine-loaded nanoparticles in Lovo cells—a possible Trojan strategy against cancer. Eur J Pharm Biopharm, 2010, 75: 334–340

42 Huang Z, Zhang L, Duan X, Liao Z, Ding H, Cheung PCK. Novel highly branched water-soluble heteropolysaccharides as immunopotentiators to inhibit S-180 tumor cell growth in BALB/c mice. Carbohyd Polym, 2012, 87: 427–434

43 Xu L, Chen H, Xu H, Yang X. Anti-tumour and immuno-modulation effects of triptolide-loaded polymeric micelles. Eur J Pharm Biopharm, 2008, 70: 741–748

44 Vezmar S, Becker A, Bode U, Jaehde U. Biochemical and clinical aspects of methotrexate neurotoxicity. Chemotherapy, 2003, 49: 92–104

45 Jiang Y, Jiang X, Law K, Chen Y, Gu J, Zhang W, Xin H, Sha X, Fang X. Enhanced anti-tumor effect of 9-nitro-camptothecin complexed by hydroxypropyl-beta-cyclodextrin and safety evaluation. Int J Pharm, 2011, 415: 252–258

46 Chau Y, Padera RF, Dang NM, Langer R. Antitumor efficacy of a novel polymer-peptide-drug conjugate in human tumor xenograft models. Int J Cancer, 2006, 118: 1519–1526

47 Zhu L, Huo Z, Wang L, Tong X, Xiao Y, Ni K. Targeted delivery of methotrexate to skeletal muscular tissue by thermosensitive magnetoliposomes. Int J Pharm, 2009, 370: 136–143

Supporting Information

Figure S1 Optical micrographs of MG-63 cells cultured for 72 h (×100) with fresh medium (control) (A); 100 μg mL^{-1} MCMs (B); 3 μg mL^{-1} MTX (C); 3 μg mL^{-1} MTX nanoparticles (D); 3 μg mL^{-1} MMCMs (C) (E); 3 μg mL^{-1} MMCMs (M) (F).

Figure S2 Prussian blue staining of tumor in S-180 bearing mice (×300): (A) blank control; (B) MTX; (C and D) MMCMs (C/M) at the dose level of 10 mg kg^{-1} under magnetic induction.

The supporting information is available online at life.scichina.com and link.springer.com. The supporting materials are published as submitted, without typesetting or editing. The responsibility for scientific accuracy and content remains entirely with the authors.